Organometallic Deposition of Ultrasmooth Nanoscale Ni film

András Paszternák[1,2]*, Meital Shviro[1] and David Zitoun[1]*

[1] Bar Ilan University, Department of Chemistry and Bar Ilan Institute of
Nanotechnology and Advanced Materials (BINA), Ramat Gan 52900, ISRAEL

[2] Institute of Materials and Environmental Chemistry, Research Centre for Natural
Sciences, Hungarian Academy of Sciences, 1117 Budapest,
Magyar tudósok körútja 2., HUNGARY

david.zitoun@biu.ac.il

paszternak.andras@ttk.mta.hu

ABSTRACT

Deposition of nanoscale and smooth Ni film is challenging using wet chemistry. Herein, organometallic Ni precursor yields colloidal nanoparticles which self-assemble into thin metallic film with uniform thickness on large scale. More precisely, we report on the one-pot synthesis and self-assembly of a monolayer of amorphous Ni nanoparticles on areas as large as $10\ \mu m^2$, with a thickness as low as 10 nm and a roughness of 1.1 nm (RMS). Interestingly, the reactivity of different complexes, whether organometallic (OM), namely Ni $(\eta^4–C_8H_{12})_2$ or metal-organic (MO), namely Ni(acac)$_2$, orthogonally depends on whether the reaction is performed on a silicon wafer or in solution. Only the combination of phosphine and amine ligands with OM precursor effectively controls the homogeneity of the film on large scale, while phosphine ligands result in P doping of the amorphous Ni.

KEYWORDS: nickel, electroless deposition, magnetism, thin film, coating

INTRODUCTION

Thin films of Ni have been extensively studied for their magnetic, catalytic and electronic properties. Physical deposition methods, like sputtering, are widely viewed as the most common pathway towards low roughness and grain size Ni thin films (Priyadarshini et al. 2011). Wet chemistry deposition methods like the classical electroless deposition method yield much thicker film (Schlesinger 2010). Referring specifically to electroless nickel deposition, hypophosphite generally results in high phosphorous content (Ni – P alloys with 3 to 35 P atomic percent, depending on the experimental conditions, solution composition and pH) (Bard et al. 2012)).

Self-assembly of Ni nanoparticles (NPs) in a thin film presents the appealing advantage of being adjustable to their nominal size. Ni NP can be synthesized in alkylamines used as solvents, surfactants and reducing agents (Mourdikoudis et al. 2009). The use of phosphorous containing ligands like trialkylphosphine with metal-organic Ni(acetylacetonate)$_2$ {Ni(acac)$_2$} is the most common method for monodisperse Ni nanoparticle formation (Moreau et al. 2012; Chen et al. 2010). These coordinating molecules play a crucial role in controlling the size and morphology of the nanoparticles, stabilizing the nanoparticles, and coordinating the precursors. Trioctylphosphine oxide (TOPO) is also used by many research groups in the presence of alkylamines (Hou et al. 2005; Luo et al. 2009; LaGrow et al. 2012). Thermal decomposition of metal-organic (MO) nickel complexes (like cupferrates) in a mixture of octylamine/octadecene with different volume ratios forms various morphologies of oxidized nickel structures (Diab et al. 2012). This route involves a two-step process with the synthesis of monodisperse NPs and their self-assembly in a monolayer.

On the other hand, examples of one-pot formation of nanoparticles layers have been published for other metals like Cu NPs; closed packed layers of Cu NPs spontaneously form in surfactant mixtures (phosphine/amine) (Diab et al. 2011). The amine component has two important roles, as a reducing agent and as a surfactant for determining the morphology and assembly of NPs. However, a thick (0.1–7 μm) organic layer has been observed between the metallic layer and the underlying silicon substrate on cross-sectional SEM images. Attempts to remove this buffer layer via solvent washings disrupt the continuity of the formed metallic layer, which impedes

the practical use of this method. The use of organometallic (OM) precursor has been very successful to yield thick continuous Cu thin film with high electrical conductivity (Barrière et al. 2008). Organometallic (OM) nickel deposition from Ni(Cyclooctadiene)$_2$ [Ni(COD)$_2$ or Ni (η^4–C$_8$H$_{12}$)$_2$] has been previously reported from a surfactant free solution; thin film grows by self-assembly of polydisperse crystalline Ni NPs with grain size of about 10 nm (Shviro et al. 2012). The film consists of polydisperse NPs which form 2D or 1D nanostructures without any template (Shviro et al. 2013).

Following our work on surfactant-free organometallic decomposition and the interest in controlling both the self-assembly and phosphorous doping of Ni thin films, we investigate in the present manuscript a facile one-step synthesis of self-assembled monodisperse Ni NPs using a mixture of surfactants (alkylamines and trialkyl phosphines). We report on the synthesis and self-assembly of a monolayer of Ni nanoparticles on very large scale (> 10 μm^2) with a very low roughness (RMS ~ 1.1 nm). The reactivity of different complexes (MO Ni(acac)$_2$ or OM Ni (η^4–C$_8$H$_{12}$)$_2$) orthogonally depends on whether the reaction is performed on a silicon wafer or in solution. Nanoparticles and thin nickel layers are fully characterized by SEM, EDAX, TEM, AFM, XPS and SQUID.

EXPERIMENTAL PROCEDURE

Ni thin film elaboration:

Silicon (Virginia semiconductors, <100>, n-type, 4-6 Ω.cm) substrates were washed, covered with a monolayer using octadecyltrichlorosilane (Aldrich, 97%) according to a standard procedure (Wang and Jin 2004). 5 mg of Ni (η^4–C$_8$H$_{12}$)$_2$ or Ni(acac)$_2$ were dissolved in the mixture of trioctylphosphine (TOP, 97%): octadecylamine (ODA, 90%) /ratio 10:1/. In a typical experiment, the solution was drop-casted on the functionalized Si wafer in a glovebox. The coating was then annealed on a heating plate or in an oven at 120 ºC for 15 min and at 240 ºC for 15 minutes in inert atmosphere.

Ni colloidal dispersion preparation:

Ni (η^4–C_8H_{12})$_2$ (STREM, 98%), Ni(acac)$_2$ (STREM) were stored in a glovebox. The Ni nanoparticles were prepared by the decomposition of Ni(acetylacetonate)$_2$ (2.0 mmol), oleylamine (6.0 mmol) with trioctylphosphine (11.2 mmol) under nitrogen atmosphere for 30 min at 215 ˚C (Park et al. 2005). Ni (η^4–C_8H_{12})$_2$ (0.12 mmol) was dissolved in trioctylphosphine (0.89 mmol) and mesitylene (3 mL) and heated under nitrogen for 30 min at 170˚C.

AFM:

The morphology of the coating was studied using an Atomic Force Microscope (AFM, ICON, Bruker) in tapping mode with a silicon nitride tip (FESP).

TEM and SEM:

HRSEM images were collected on a FEI Magellan equipped with an Energy-Dispersive X-ray (Oxford 80 mm^2) spectroscopy attachment. EDAX has been typically collected on images of 25 μm^2 to provide a statistical analysis on different regions and a reliable composition.

Cross section of the coating on the Si surface was achieved using a Helios 600, dual beam FIB instrument. The cross section was connected with a thick layer of platinum to the corner of a TEM grid for HRTEM analysis (JEOL JEM 2100). Samples prepared on TEM grid were checked on a JEM-1400 microscope from JEOL.

SQUID:

Magnetic properties were measured using a Superconducting Quantum Interference Design (SQUID) magnetometer MPMS XL7, in the range of temperature 2-300 K and of field 0-5 T. The temperature-dependent susceptibility was measured using DC procedure. The sample was transferred under nitrogen to the SQUID chamber to prevent any oxidation. The sample was cooled to 2.0 K under zero magnetic field, low magnetic field (5.0 mT) was applied and data collected from 2 K to 300 K (zero-field cooled, ZFC). Field Cooled (FC) measurements were performed from 2K to 300K with an applied field during the cooling. Hysteresis loop was measured at 2 K.

XPS:

Measurement was performed with a Kratos axis HS spectrometer. Data manipulation and interpretation was carried out with OEM Vision 2 software.

RESULTS AND DISCUSSIONS

Layer of closely packed nickel nanoparticles with uniform size distribution is formed on top of silicon substrate treated with octadecyltrichlorosilane (OTS) after drop-casting and thermal decomposition of Ni $(\eta^4–C_8H_{12})_2$ precursor dissolved in mixture of trioctylphosphine (TOP) and octadecylamine (ODA) (Fig. 1). The average grain size of nickel particles is 16.3 ± 2.9 nm based on HRSEM image analysis. Nanoparticles self-assemble into 50 nm islands with short line defects between them. In Fig. 1C, HRSEM clearly shows each particle as individual and most probably surrounded with surfactants. The defects do not extend more than several nm wide and tens of nanometers long. The percolation between the islands yields homogeneous layer on several micron square (Fig. 1A). Such an assembly usually results from slow ordering of particles at solid/liquid interface (Guo et al. 2003). On top of this layer, some areas are still covered with organic residues which can be reduced by further washing and vacuum treatments.
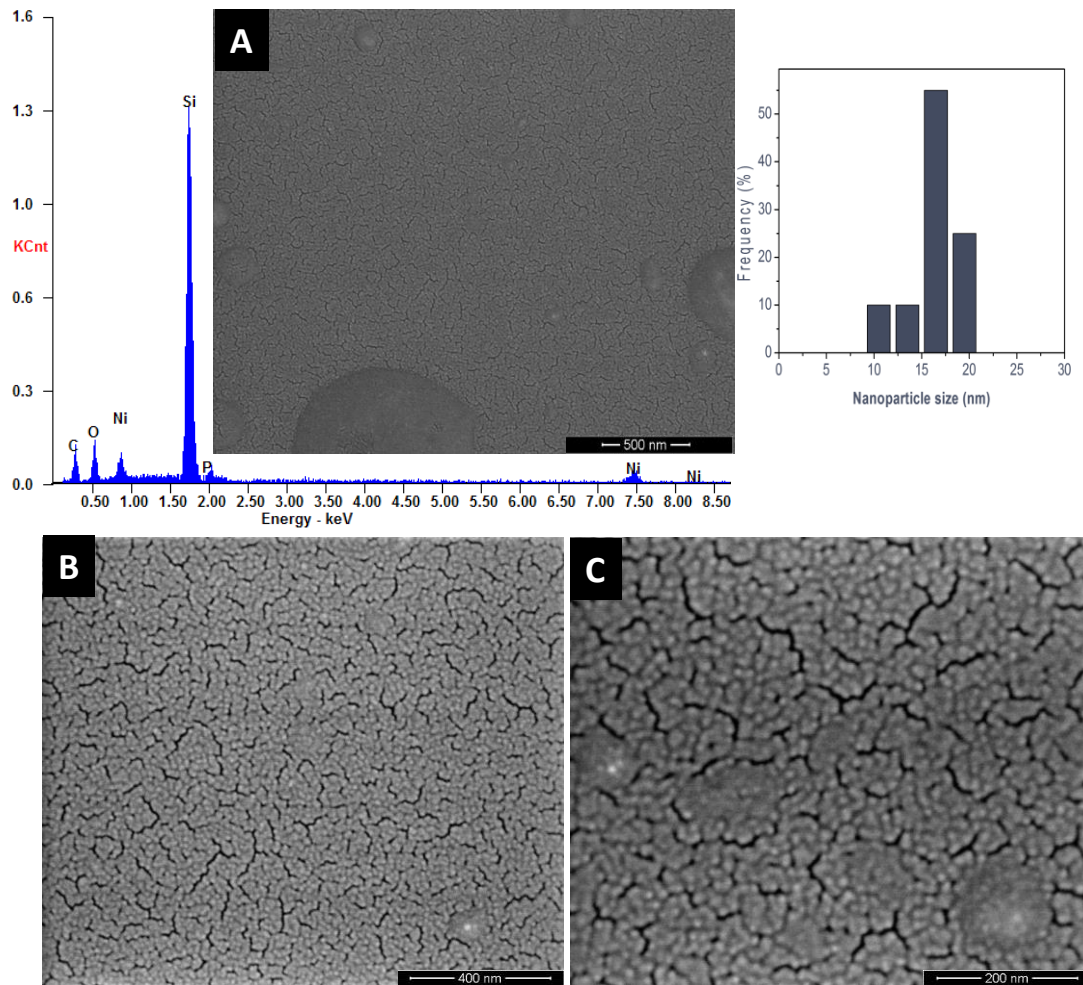
Figure 1: SEM image of nickel thin layer with EDAX spectrum (A); HRSEM images of Ni Layer with corresponding size histogram of Ni grain size (B, C)

The EDAX results confirm the presence of Ni in the film (8 %(w.)). Phosphorous is also present in the layer (1.5 %(w.)) (Fig. 2). The two elements are homogeneously dispersed in the film (Fig. 2B and 2D). Based on the literature P insertion from TOP ligands into Ni nanoparticles can change the properties of the products and also have an important impact on the possible future applications (Moreau et al. 2012). Phosphorous is thought to act as an inhibitor of crystallization; P atoms are trapped between the nickel atoms and their presence reduces the possibility of metallic bonding necessary for crystal growth (Schlesinger 2010).
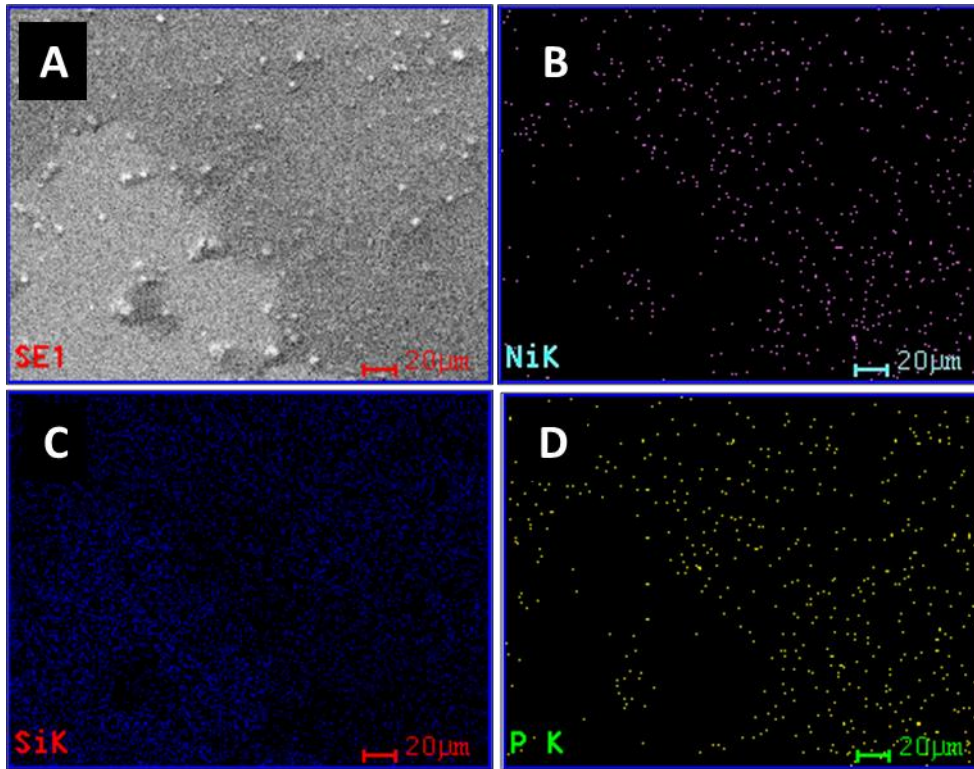
Figure 2: EDAX map at the Ni-layer/substrate border, showing the presence of phosphorous all over the layer (A – SEM image, B – Ni map, C – Si map, D – P map)

Atomic force microscope (Fig. 3) is used to get detailed information about the layer formed by nanoparticles. The layers, measured in tapping mode, presents a good adhesion to the silicon wafer. The average particle size is 23.6 ± 3.9 nm based on AFM image analysis.
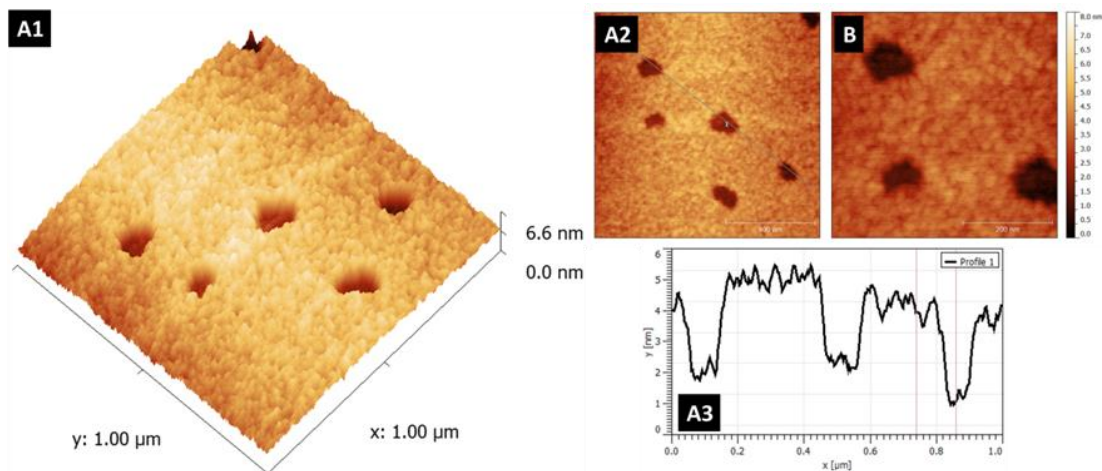
Figure 3: AFM images of Ni layer 1 μm^2 (A1); corresponding 2D display (A2); selected 0.25 μm^2 (B); cross-section profile from A2 (A3)

The morphology of the surface exhibits relatively large smooth areas. The surface roughness of Ni layer is calculated as the Root Mean Square RMS ~ 1.1 nm. As a comparison, we have measured the average roughness of a sputtered nickel layer on the same Si wafer and found out a value of RMS~2-3 nm (depending on the parameters used for the preparation). On the other hand, when the organometallic Ni precursor is spin-coated and thermally decomposed at temperature between 80 and 150°C (Shviro et al. 2012), the layer displays a roughness RMS ~3-4 nm. The layers are extremely smooth compared to any other electroless or sputtering deposition techniques. From the typical cross section analysis profile of the image (Fig. 3A3), one can calculate the depth of the holes in the layer to be at least 3 nm. This value stands as a lower value of the layer thickness and does not account for the real layer thickness since we do not observe evidence that the bottom of the hole corresponds to the substrate or to the layer itself.

Therefore, we perform a cross section of the coating using a dual beam FIB instrument to measure the sample thickness. The Ni layer is connected with a thick layer of platinum to the corner of a TEM grid for HRTEM analysis (Fig. 4). On figure 4, from right to left, one can distinguish the Si wafer (grey), SiO_2 native oxide (light grey), Ni film (dark grey) and Pt (textured material). Based on HRTEM image, the thickness of the nickel layer is around 10 ± 1 nm. The nickel layer is amorphous according to the selected area electron diffraction (SAED) and the Fourier transform of all HRTEM images (not shown). XRD also confirms the amorphous nature of the layer (not shown). The formation of amorphous Ni layer can be explained also thanks to the presence of P impurities. As discussed above, P can act as an inhibitor of crystal formation (Schlesinger 2010).
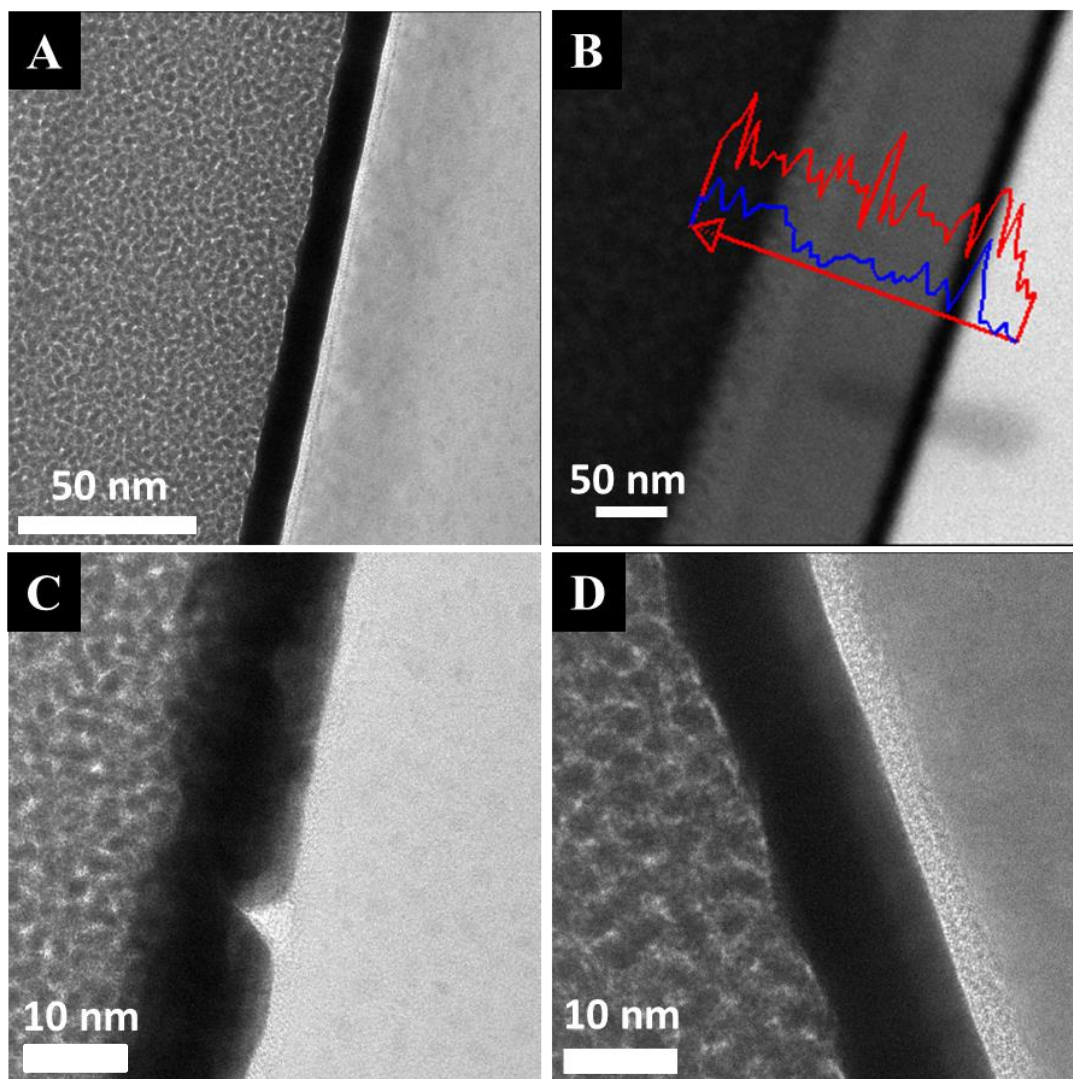
Figure 4: TEM images of the layer cross-section (A); TEM image with EDAX profile analysis (O: red, Ni: blue) (B); HRTEM images on two different locations of the film (C, D)

The same experiment is repeated on a TEM grid (silicon monoxide Type-A, 300 mesh) to monitor directly the thermal decomposition of metallic precursor and the formation of Ni nanoparticles, forming the thin layer as discussed above. The chemical nature of the surface (SiO) is close to the native oxide on the Si wafer, but displays a higher roughness and a curvature from the Cu mesh supporting the SiO. The reaction yields aggregates of amorphous nanoparticles without percolation as observed by TEM on Fig. 5.
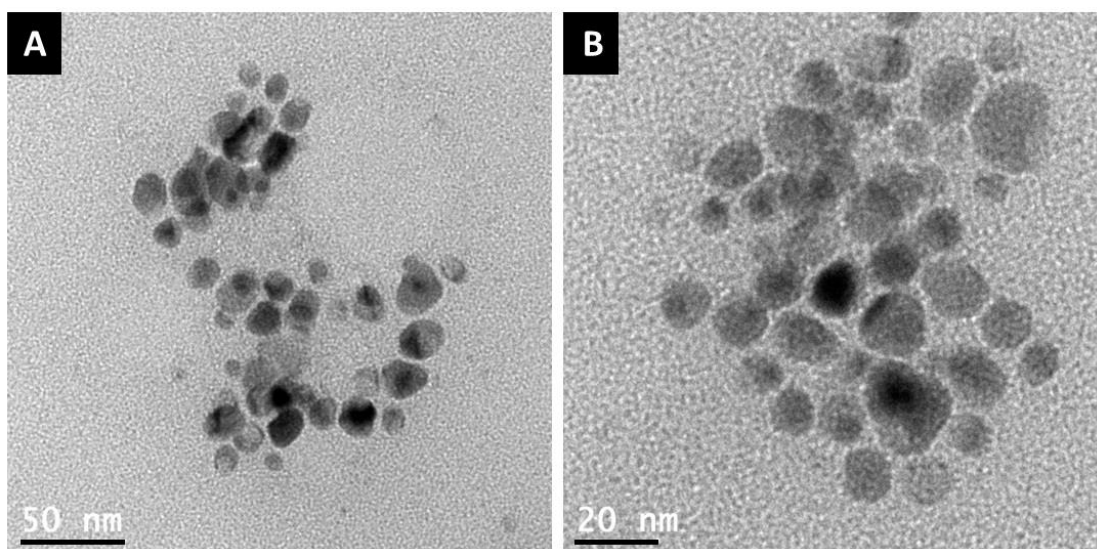
Figure 5: TEM image of the Ni nanoparticles prepared in-situ on TEM grid

The average size of the particles is 15.6 ± 3.2 nm, which is in good correspondence with results obtained by HRSEM (16.3 ± 2.9 nm), AFM (23.6 ± 3.9) and HRTEM images of the cross-section (10 ± 1 nm) of the Ni film. The amorphous character of the nanoparticles is consistent with the diffractions collected on the thin film.

To get detailed information about the layer structure and composition, we measure X-Ray Photoelectron Spectroscopy (XPS). XPS confirms the presence of nickel in the layer. The whole spectrum and the energy range corresponding to Ni 2p are presented on Fig. 6. The Ni 2p peaks display a complex feature which can be fitted by several contributions. The broad peak at 862 eV corresponds to a satellite of the main peak at 856 eV. The low energy contribution at 854 eV (blue Gaussian on Fig. 6B) corresponds to low oxidation Ni (either Ni(0) or nickel phosphide). Based on the literature, the typical binding energy signals of Ni 2p are 853.5 eV for Ni_2P (Panneerselvam et al. 2007) and 852.9 eV for Ni_3P (Elsener et al. 2008). The two contributions at 856 eV and 857 eV can be assigned to Ni (II) species, either layer's surface atoms coordinated by amine or phosphine. Due to the non-univocal assignation of the contribution in Ni $2p_{3/2}$ peaks, ascribing the spectral feature to a specific compound is difficult, as usual for transition metals.
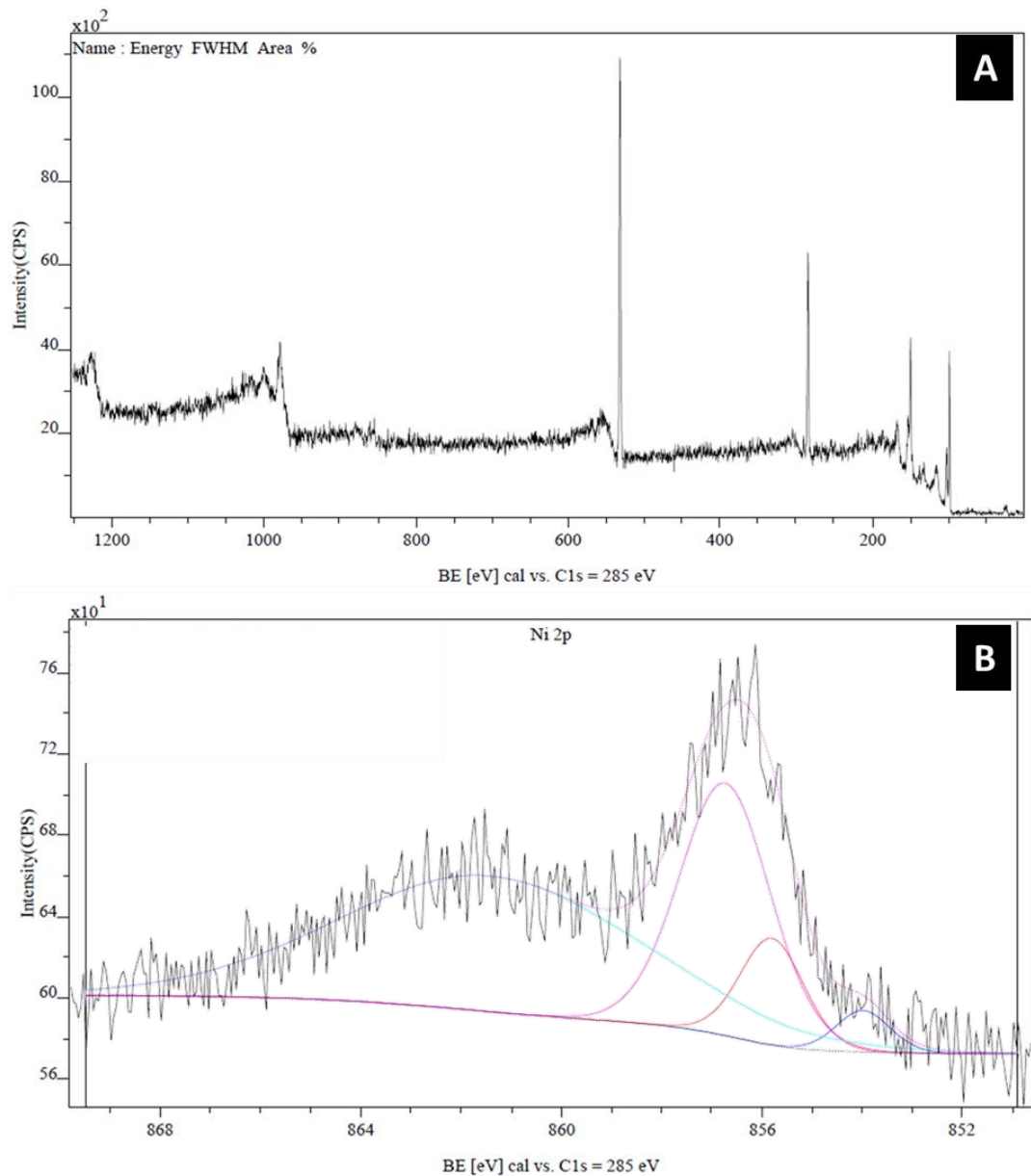
Figure 6: XPS spectra of the nickel layer (A); Energy range corresponding to the Ni $2p_{3/2}$ transitions with spectrum fit (purple) and all contributions (see text) (B)

Magnetic measurements on the sample have been performed using a SQUID magnetometer. Two sets of experiments are needed to evaluate the quality of the film. First, low temperature hysteresis are measured on the sample (Fig. 7A). The magnetic measurements are collected on $5*5$ mm^2 samples with a non-saturating magnetization in the 10^{-3} μ_B range and no coercitive field. We have then measured the temperature dependence of the magnetization following a zero-field-cooled/field-cooled (ZFC/FC) measurement from 2 K to 300 K with an external field $\mu_0H = 0.005$ T (Fig. 7B). The layer mainly displays a paramagnetic behavior with a hysteresis observed on all the

temperature range. This behavior is typically observed for spin-glass materials with high degree of disorder. This model is consistent with an amorphous P doped Ni thin film.
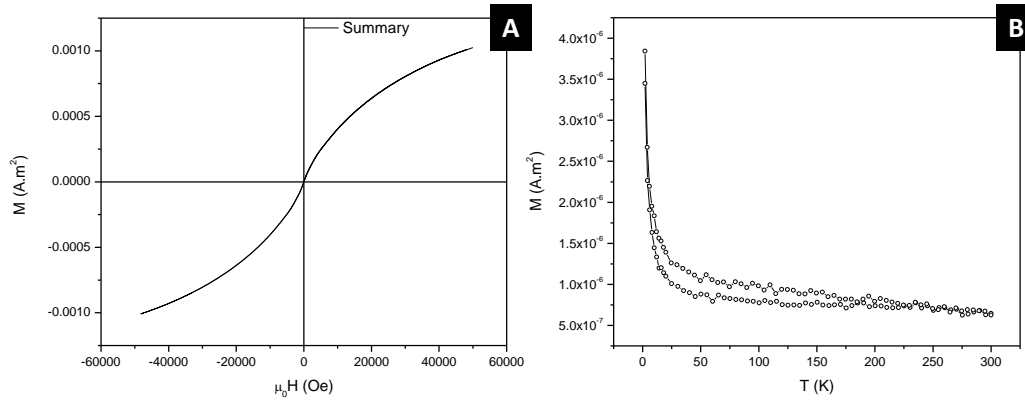

Figure 7: Magnetization data for nickel layer: hysteresis loop at T = 2 K (A) and ZFC/FC at $\mu_0 H = 0.005$ T (B).

Since we have observed significant differences between the reaction on Si wafer surface and in solution, we investigate the use of a classical Ni precursor (Ni(acetylacetonate)$_2$ or Ni(acac)$_2$) extensively used in the literature. Layer formation process is repeated using anhydrous Ni(acac)$_2$ instead of Ni (η^4–C$_8$H$_{12}$)$_2$. As observed on Figure 8, the reaction yields an inhomogeneous layer (Fig. 8B) compared to the organometallic precursor Ni (η^4–C$_8$H$_{12}$)$_2$. Ni amount measured by EDAX is significantly lower [0.1 %(w.) for Ni(acac)$_2$ vs 8.0 %(w.) for Ni (η^4–C$_8$H$_{12}$)$_2$].
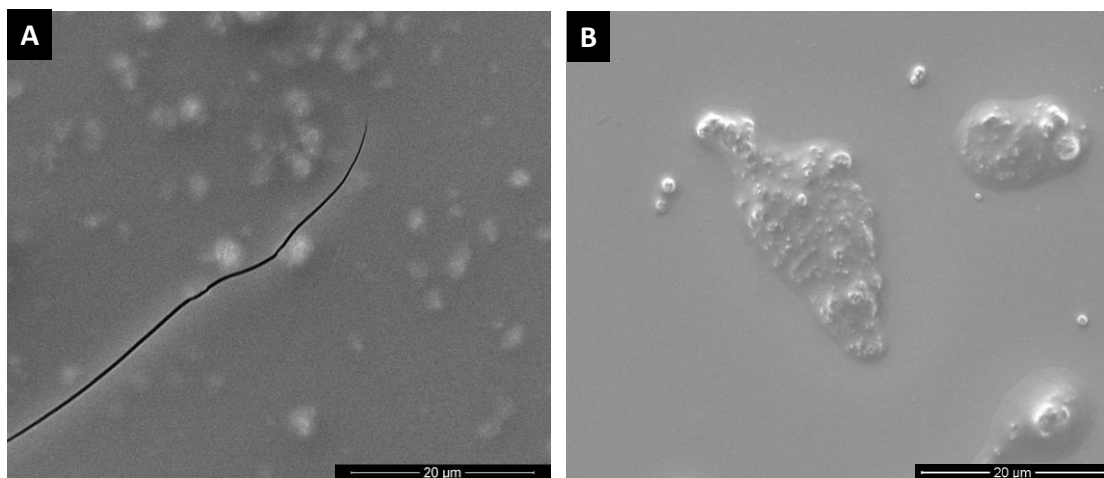
Figure 8: SEM image of the thin layer prepared with Ni (η^4–C$_8$H$_{12}$)$_2$ (A) and Ni(acac)$_2$ (B)

12

Ni nanoparticle synthesis in solution

To confirm these results, we have performed the synthesis of Ni nanoparticles in solution using either the organometallic precursor Ni $(\eta^4-C_8H_{12})_2$ or metal-organic Ni(acac)$_2$.

The synthesis from metal-organic Ni(acac)$_2$ is reported in the literature (Park et al. 2005). The Ni nanoparticles are prepared by the decomposition of Ni(acac)$_2$-oleylamine complex with trioctylphosphine under nitrogen atmosphere for 30 min at 215˚C. This procedure results in the formation of 3 nm sized nickel nanoparticles (Fig. 9). The sample does not display any electron or X-Ray diffraction. The detailed study of the reaction has been highlighted recently showing the large P doping resulting in the highly disordered structure (Moreau et al. 2012).
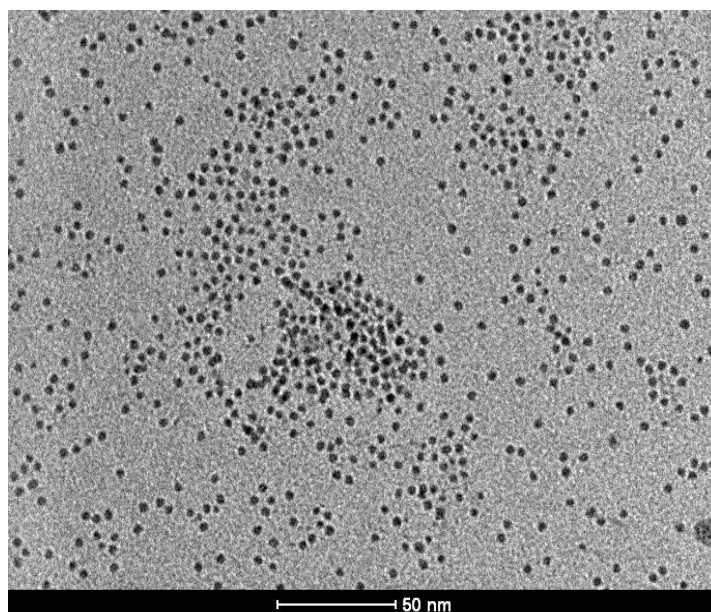

Figure 9: TEM of Ni nanoparticles synthetized from Ni(acetylacetonate)$_2$

When the same reaction is performed with the organometallic Ni $(\eta^4-C_8H_{12})_2$, the yellow solution turns dark red and does not evolve after prolonged heating. Diffusion Light Scattering measurement shows no scattering and no precipitate could be obtained after repeated centrifugation. The product should be a trioctylphosphine complex of Ni which does not decompose upon heating. The reaction is specific to TOP ligands since amines ligands yield Ni nanocrystals with define shapes (Shviro and Zitoun 2013). The reactivity of Ni(acac)$_2$ and Ni $(\eta^4-C_8H_{12})_2$ orthogonally depends on whether the reaction is performed on a silicon wafer or in solution.

CONCLUSION

The direct decomposition of organometallic precursor on surfaces has yielded highly smooth film (1.1 nm RMS for a 10 nm thick film) on a very large scale (10 μm^2). The film is formed by self-assembly of 16 nm wide and 10 nm thick nanoparticles with very few line defects. The film is amorphous with a high content of phosphorous and behaves like a magnetic spin glass. A drastic change is found on the nickel nanoparticles formation by exchanging the organometallic Ni (η^4–C_8H_{12})$_2$ with metal-organic Ni(acac)$_2$ precursor. The formation of a homogeneous film occurs only with the organometallic precursor. On the other hand, monodisperse Ni:P nanoparticles are formed by reacting metal-organic Ni(acac)$_2$ while organometallic Ni (η^4–C_8H_{12})$_2$ yields a stable complex.

Based on this result we can conclude that the substrate surface has an important role for the *in situ* layer synthesis and promotes reaction which does not occur in solution. The resulting thin film displays smoothness and homogeneity above the state of the art techniques.

References:

Bard AJ, Inzelt G, Scholz F (2012) Electrochemical Dictionary, 2nd edn. Springer, London – New York, pp 299-300

Barrière C, Alcaraz G, Margeat O, Fau P, Quoirin JB, Anceau C, Chaudret B (2008) Copper nanoparticles and organometallic chemical liquid deposition (OMCLD) for substrate metallization. J Mater. Chem. 18:3084

Chen D-X, Pascu O, Roig A, Sanchez A (2010) Size analysis and magnetic structure of nickel nanoparticles. Journal of Magnetism and Magnetic Materials 322: 3834-3840

Diab M, Moshofsky B, Jen-La Plante I, Mokari T (2011) A facile one-step approach for the synthesis and assembly of copper and copper-oxide nanocrystals. J. Mater. Chem. 21:11626-11630

Diab M, Volokh M, Moshofsky B, Jen-La Plante I, Flomin K, Chockler E, Mokari T (2012) A Simple Approach for the Formation of Oxides, Sulfides, and Oxide–Sulfide Hybrid Nanostructures. Isr. J. Chem. 52:2723-2728

Elsener B, Atzei D, Krolikowski A, Rossia A (2008) Effect of phosphorus concentration on the electronic structure of nanocrystalline electrodeposited Ni–P alloys: an XPS and XAES investigation. Surf. Interface Anal. 40: 919-926

Guo Q, Teng X, Rahman S, Yang H (2003) Patterned Langmuir-Blodgett Films of Monodisperse Nanoparticles of Iron Oxide Using Soft Lithography. J. Am. Chem. Soc.125:630-631

Hou Y, Kondoh H, Ohta T, Gao S (2005) Size-controlled synthesis of nickel nanoparticles. Applied Surface Science 241:218–222

LaGrow AP, Ingham B, Cheong S, Williams, GVM, Dotzler Ch, Toney MF, Jefferson DA, Corbos EC, Bishop PT, Cookson J, Tilley RD (2012) Synthesis, Alignment, and Magnetic Properties of Monodisperse Nickel Nanocubes. J. Am. Chem. Soc. 134:855−858

Luo X, Chen Y, Yue G-H, Peng D-L, Luo X (2009) Preparation of hexagonal close-packed nickel nanoparticles via a thermal decomposition approach using nickel acetate tetrahydrate as a precursor. Journal of Alloys and Compounds 476: 864–868

Moreau LM, Ha D-H, Bealing CR, Zhang H, Hennig RG, Robinson RD (2012) Unintended Phosphorus Doping of Nickel Nanoparticles during Synthesis with TOP: A Discovery through Structural Analysis. Nanoletters 12:4530-4539

Mourdikoudis S, Simeonidis K,Vilalta-Clemente A, Tunab F, Tsiaoussis I, Angelakeris M, Dendrinou-Samara C, Kalogirou O (2009) Controlling the crystal

structure of Ni nanoparticles by the use of alkylamines. Journal of Magnetism and Magnetic Materials 321:2723–2728

Panneerselvam A, Malik MA, Afzaal M, O'Brien P, Helliwell M (2007) The Chemical Vapor Deposition of Nickel Phosphide or Selenide Thin Films from a Single Precursor. J. Am. Chem. Soc.130:2420-2421

Park J, Kang E, Son SU et al (2005) Monodisperse Nanoparticles of Ni and NiO: Synthesis, Characterization, Self-Assembled Superlattices, and Catalytic Applications in the Suzuki Coupling Reaction. Adv. Mater.17:429-434

Priyadarshini BG, Aich S, Chakraborty M (2011) Structural and morphological investigations on DC-magnetron-sputtered nickel films deposited on Si (100). J Mater Sci 46:2860–2873

Schlesinger M (2010) Electroless deposition of Nickel. In: Modern electroplating, Wiley, New York, pp 447-457

Shviro M, Zitoun D (2012) Low temperature, template-free route to nickel thin films and nanowires. Nanoscale 4:762-767

Shviro M, Paszternák A, Chelly A, Zitoun D (2013) Zigzag-shaped nickel nanowires via organometallic template-free route. Journal of Nanoparticle Research15:1823

Shviro M, Zitoun D (2013) Nickel nanocrystals: fast synthesis of cubes, pyramids and tetrapods. RSC Adv. 3:1380-1387

Wang Z-H, Jin G (2004) Silicon surface modification with a mixed silanes layer to immobilize proteins for biosensor with imaging ellipsometry. Colloids and Surfaces B: Biointerfaces 34:173-177